Breaking Force and Conductance of Gold Nanojunctions: Effect of Humidity

ARTICLE *in* JOURNAL OF PHYSICAL CHEMISTRY LETTERS · OCTOBER 2014

Impact Factor: 7.46 · DOI: 10.1021/jz5019459

6 AUTHORS, INCLUDING:

Miklós Mohos
Universität Bern
7 PUBLICATIONS **18** CITATIONS
SEE PROFILE

Ilya Pobelov
Universität Bern
40 PUBLICATIONS **968** CITATIONS
SEE PROFILE

Viliam Kolivoska
Academy of Sciences of the Czech Republic
42 PUBLICATIONS **273** CITATIONS
SEE PROFILE

THE JOURNAL OF PHYSICAL CHEMISTRY Letters

Letter

pubs.acs.org/JPCL

Breaking Force and Conductance of Gold Nanojunctions: Effect of Humidity

Miklós Mohos,[†] Ilya V. Pobelov,*[,†] Viliam Kolivoška,[†,‡] Gábor Mészáros,[†,¶] Peter Broekmann,[†] and Thomas Wandlowski[†]

[†]Department of Chemistry and Biochemistry, University of Bern, Freiestrasse 3, 3012 Bern, Switzerland

[‡]J. Heyrovský Institute of Physical Chemistry of ASCR, v.v.i., Dolejškova 3, 18223 Prague, Czech Republic

[¶]Institute of Materials and Environmental Chemistry, Research Centre for Natural Sciences, Hungarian Academy of Sciences (HAS), Magyar tudósok körútja 2, H-1117 Budapest, Hungary

ABSTRACT: Forces acting on elongated gold nanojunctions and their electric conductance were simultaneously measured by current-sensing force spectroscopy in an atmosphere with controlled humidity. The breaking force of "thick" nanojunctions with conductance >20G_0 is not affected by the environmental humidity. The presence of ambient water stabilizes "thin" nanojunctions with conductance <15G_0, whose breaking force of 10−15 nN was higher than that in a dry atmosphere due to the capillary forces. The observed effect of humidity would not be possible to distinguish by techniques measuring only forces or only conductance in nanojunctions.

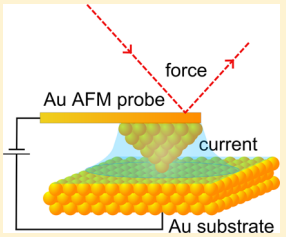

SECTION: Surfaces, Interfaces, Porous Materials, and Catalysis

The adsorption of water tremendously affects the mechanical properties of surfaces and interfaces,[1,2] as well as the forces acting between them.[3] The latter are commonly probed at the nanoscale by force−distance spectroscopy carried out in an atomic force microscopy (AFM) configuration.[4−6] In vacuum, dry gaseous environment, or the liquid phase, the adhesion force F_{adh}, that is, the force required to detach an AFM probe from a sample surface, may be represented as a sum of electrostatic F_{el}, van der Waals F_{vdW}, and chemical F_{chem} contributions, accounting for the existence of ion−ion, dipole−dipole, and specific (e.g., receptor−ligand) interactions, respectively.[5] In a gaseous phase containing water vapor, for example, under ambient conditions, water adsorbed on the surfaces may lead to the formation of a water neck between the probe and the substrate.[7−14] Therefore, an additional capillary force F_{cap} needs to be taken into account.[5] The magnitude of the latter is affected by the structure of the water neck, which, in turn, depends on the relative humidity (RH, ratio of the partial pressure of water vapor to the pressure of saturated water vapor at the same temperature) of the environment as well as on the hydrophilicity of the AFM probe and the sample material. On hydrophilic surfaces, F_{adh} is small and rather constant at low humidities. Above a critical threshold of RH, F_{adh} exhibits a steep increase attributed to the capillary force due to the formation of the water neck.[8,11,12,15−19] After reaching a maximum, a steady decrease of F_{adh} with the further increase of RH due to the expansion of the water neck was sometimes observed.[11,15−17] On the contrary, F_{adh} was found to be rather independent of RH for hydrophobic surfaces.[16,17,19]

Besides mechanical strength, electric conductance represents another fundamental property of nanostructures that may be affected by the ambient humidity.[20,21] Mechanical and electric properties of nanocontacts can be addressed simultaneously by measuring forces and currents during the junction formation, elongation, and breaking in a current-sensing (CS) AFM (CSAFM) setup.[22] Among the different types of nanocontacts, the homogeneous metallic nanojunctions, such as those formed between the scanning probe and the sample made of or covered by the same metal, are distinguished by their basic structure. They exhibit interesting quantum effects[23] as well as serve as a reference for the characterization of molecular junctions, whose versatile properties might be employed in future molecular electronic devices.[24−26] Electric conductance and breaking forces of metallic nanojunctions have been simultaneously measured in various environments, including ultrahigh vacuum,[27] nonconductive organic solvents,[28,29] and aqueous electrolytes.[30] Although CSAFM experiments addressing metal nanocontact under ambient conditions were reported in a few works,[31−33] their authors did not take humidity into account. On the other hand, reported CSAFM experiments in an environment with a well-controlled humidity were motivated by the characterization of surface morphology and conductance, for example, in proton exchange membranes.[34−38]

In this work, we systematically studied the dependence of mechanical strength and electric conductance of homogeneous gold nanojunctions on RH. The junctions were formed by contacting an atomically flat Au(111) substrate with a gold-covered AFM probe and subsequently pulling it away from the surface. The microscope stage was housed in an environmental chamber allowing precise control of the humidity in an argon atmosphere. In order to obtain statistically significant results,

Received: September 13, 2014
Accepted: October 3, 2014

   dx.doi.org/10.1021/jz5019459 | J. Phys. Chem. Lett. 2014, 5, 3560−3564

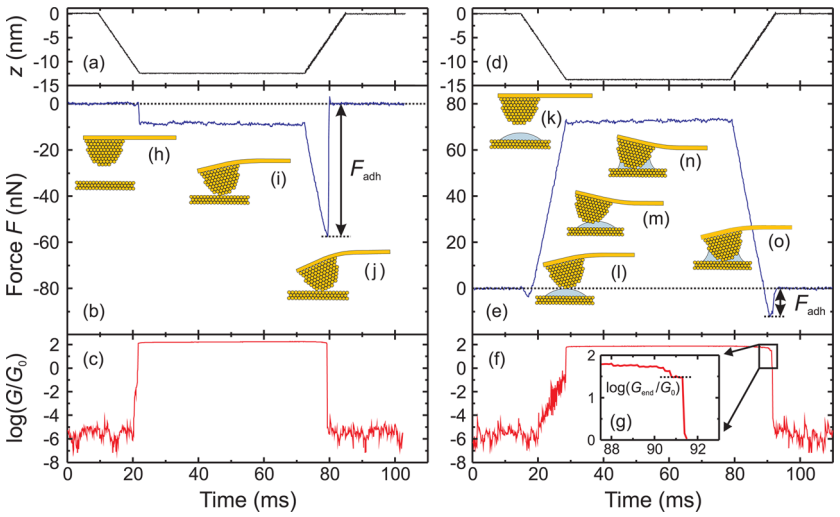

Figure 1. Probe trajectories (a,d), force (b,e), and $\log(G/G_0)$ (c,f) for representative traces of the first (a–c) and second (d–f) type. (g) Zoom in on the conductance trace (f) before the junction break. (h–o) Sketches illustrating the evolution of the junctions.

we performed for each set of conditions a few thousands probe approach–withdrawal cycles at different locations on the substrate.

Representative force and conductance traces obtained during an approach–hold–withdraw cycle are shown in Figure 1. Here and further, positive and negative force values indicate repulsive and attractive interactions between the AFM probe and the substrate, respectively; zero force corresponds to a free AFM cantilever. The junction conductance G calculated from the measured electric current I and the potential difference applied between the probe and the sample, E_{bias} = 0.1 V, varies over many orders of magnitude and is presented in the normalized logarithmic scale, $\log(G/G_0)$, where G_0 = 77.5 μS is the quantum of conductance.

Both traces (Figure 1a–c and d–f) show at the beginning intervals of a constant z = 0 nm, corresponding to the cantilever resting away from the sample surface, and, respectively, F = 0 nN and $G \approx 10^{-6}G_0$, the latter corresponding to the "baseline" conductance measured in the absence of electrical contact between the electrodes. After that, the cantilever starts to approach the surface (z decreases). When the surface is reached, the traces of the first type (Figure 1a–c) display a decrease of F to negative values, that is, the cantilever is attracted to the surface (Figure 1b). At the same time, the junction conductance suddenly increases to the values between 100 and 1000G_0 (Figure 1c), which is well above the threshold used to detect the formation of a contact between the probe and the sample (50 or 100G_0). The cantilever movement is then stopped and, after a waiting time of 50 ms, reversed (z increases). Upon the probe retraction, F decreases, while G remains rather constant. Once the junction cannot withstand the exerted force anymore, it breaks. The latter is indicated by a sharp drop of the conductance to the baseline level as well as by the relaxation of the force to zero. We note that an "overshoot" of the cantilever, that is, the rise of the deflection from negative to positive values before relaxation to zero, was often observed after the breaking of highly adhesive (F_{adh} > 30 nN) junctions.

The traces of the second type (Figure 1d–f) display upon the approach a small decrease of F, which is not accompanied by the increase of G. Upon the further approach, F increases linearly, and G increases exponentially with z. When the conductance approaches 1G_0, it increases stepwise. Often, an additional probe approach was necessary to reach the conductance threshold, causing the probe to stop. The probe withdrawal after the waiting time leads to the decrease of the force to negative values and a subsequent junction break.

Only the traces of the first type were found at low humidity (RH 1.5%), while the traces of the second type were observed in addition to the traces of the first type when the humidity exceeded a certain threshold (see further). We note that the "jump to contact", that is, a sharp increase of G due to the attractive interaction between the probe and the sample observed in the traces of the first type, was found to occur only between clean surfaces.[23] On the other hand, it was reported that a stable junction with any value of conductance may be formed in air.[39] Therefore, we attribute traces of the first and second type to the probe–sample contacts formed in the absence (Figure 1h–j) and in the presence (Figure 1k–o) of water in the junction. In the absence of water, the gold probe is attracted by the gold surface during the approach (Figure 1i) and released upon the application of higher pulling forces (Figure 1j). During the approach in the presence of water, the dry probe is attracted to the surface of the water covering the sample (Figure 1l), causing a small minimum of force. No electric contact is established at this moment. Further probe movement leads to the squeezing out of the water layer (Figure 1m) and the increase of the repulsive force. We attribute the exponential increase of the measured conductance to the electron tunneling through the water layer. The probe movement stops only after physical contact with a conductance above the threshold level is established between the probe and the sample (Figure 1n).

For all traces, we calculated the adhesion force F_{adh}, that is, the absolute value of the most negative force measured during the probe retraction (see the arrows in Figure 1b and e). The value of G measured at the same moment as F_{adh} was taken as the junction conductance just before its breaking G_{end}. The conductance of the gold junctions approximately relates to the number of gold atoms in the narrowest part of the junction N as $G \approx N \cdot G_0$ and therefore indirectly reflects its "thickness".[23] Figure 2 displays pairs of F_{adh}–G_{end} values obtained from individual force and conductance traces measured at low (RH 1.5%) and high (RH 44.0%) RH. The peaks in histograms of

dx.doi.org/10.1021/jz5019459 | J. Phys. Chem. Lett. 2014, 5, 3560–3564

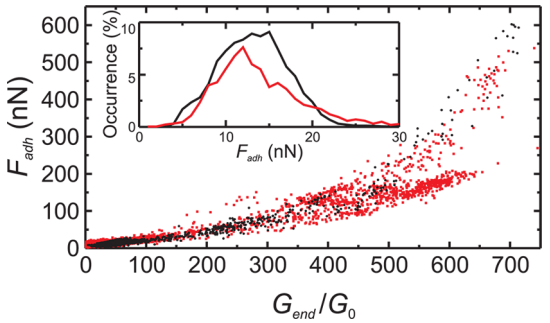

Figure 2. Pairs of F_{adh}–G_{end} values and histograms of F_{adh} (inset, bin size 1 nN) obtained from all individual traces measured at RH 1.5% (black) and RH 44.0% (red).

F_{adh} corresponding to the low and the high humidity (inset in Figure 2) demonstrate no clear difference.

The data points in Figure 2 form two trend lines displaying a faster-than-linear increase of F_{adh} with the increase of G_{end} in the range of $G_{end} > 500G_0$. The latter corresponds to 0.7 and 11.8% of all traces measured at low and high humidity, respectively. Clearly, the presence of ambient water promotes the breaking of junctions with conductance above $500G_0$ before their further evolution. One may tentatively conclude that the lower trend line is related to the ambient humidity; however, we did not identify any experimental parameter that controls the appearance of individual points in the upper or the lower trend lines.

We further concentrate on junctions with $G_{end} < 100G_0$, which constitute 93.5 and 67.0% of all traces measured at low and high humidity, respectively. We first grouped traces with $G_{end} = (N \pm 0.5)G_0$, $N = 1, 2, ..., 100$, together. The number of traces in every group divided by the total number of measured traces is shown in Figure 3a. Then, we calculated the mean value and the standard deviation of F_{adh} for every group of traces (Figure 3b). Both plots appear very similar at high G_{end} values. The occurrences of G_{end} display broad features between $15G_0$ and $90G_0$ centered at around $40G_0$. At RH 44%, almost 6% of the traces had $G_{end} < 15G_0$, while at RH 1.5%, it was only

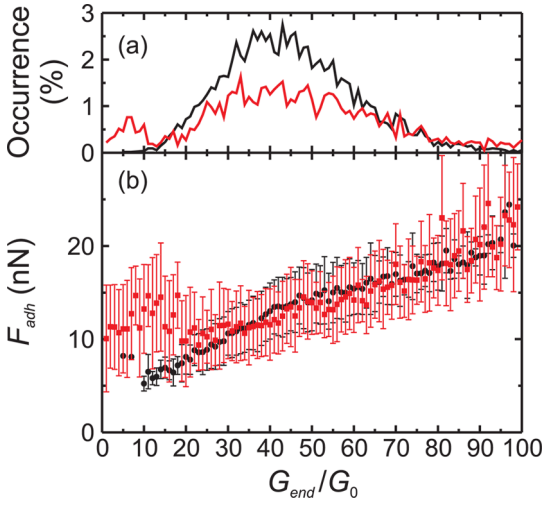

Figure 3. Relative occurrence with respect to the total number of measured traces (a) as well as the mean (symbols) and standard deviation (error bars) of F_{adh} (b) for traces with $G_{end} = (N \pm 0.5)G_0$, $N = 1, 2, ...$ measured at RH 1.5% (black) and RH 44.0% (red).

0.7% (Figure 4). The dependences in Figure 3b deviate at $G_{end} < 25G_0$; for low humidity, F_{adh} decreases linearly with the decrease of G_{end}, and for high humidity, it varies from 10 to 15 nN.

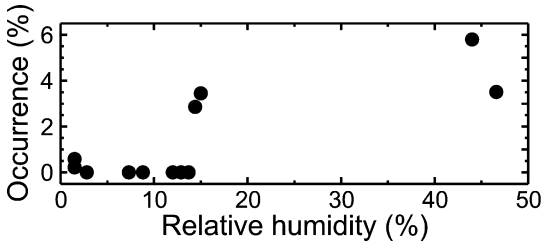

Figure 4. Occurrence of junctions with $G_{end} < 15G_0$ as a function of RH.

These observations indicate that the "thick" junctions with conductance $G_{end} > 20G_0$ reflect the intrinsic characteristics of the contact formed between the AFM probe and the gold surface. Such junctions may be (partially) covered by the water film, which did not yet develop into a complete water neck and therefore do not affect the observed junction properties. These junctions provide a major contribution to the histograms of F_{adh} (inset in Figure 2). On the other hand, "thin" gold junctions with $G_{end} < 15G_0$ are stabilized by the presence of water in the nanogap. This conclusion is also confirmed by the higher occurrence of traces of the second type, which we associate with the junctions formed and broken in the presence of water, at high humidity. All traces with $G_{end} < 10G_0$, 85% of traces with $10G_0 < G_{end} < 15G_0$, 49% of traces with $15G_0 < G_{end} < 20G_0$, and 4% of traces with $20G_0 < G_{end} < 50G_0$ were of the second type, whereas all traces with $G_{end} > 50G_0$ were of the first type. We suggest that the thin junctions are stabilized by a fully developed water neck, whose mechanical strength determines the adhesion. The adhesion force of 10–15 nN obtained for thin junctions thus can serve as an upper estimation of the force required to break the water neck formed under our experimental conditions, that is, the capillary force.

To further evaluate the effect of humidity on the gold nanojunctions, we repeated the CSAFM experiments at other RH values and calculated for every measured data set the occurrence of traces with $G_{end} < 15G_0$ (Figure 4). No thin junctions were formed at RH < 14%. Above this value, we observed a sharp rise of occurrence. We note that such humidity dependences were found for other systems and were associated with the formation of water islands on the surface.[8,11,12,15−19]

Finally, we would like to stress that it would not be possible to come to the conclusions drawn in this work in separate studies of adhesion forces or junction conductances. The histograms of adhesion forces (inset in Figure 2), as one would obtain in a generic force spectroscopy experiment,[4−6] are dominated by the contribution of the thick junctions, whose properties appear to be unaffected by humidity. The histograms of G_{end} values obtained in our experiments (Figure 3a) do show an effect of humidity; however, its attribution to the presence of water in the junction would be rather speculative without the complementary force measurements. Moreover, tip-shaped probes employed in break-junction-type experiments[24−26] are much stiffer than cantilevers used in AFM experiments.[23] They exhibit different dynamics upon the elongation of the

dx.doi.org/10.1021/jz5019459 | J. Phys. Chem. Lett. 2014, 5, 3560−3564

nanojunction. In particular, the higher probe stiffness leads to the formation of a higher number of junctions with conductance $G = G_0$ under otherwise the same conditions.[28] The results of break-junction experiments are typically analyzed by constructing histograms of all conductance values measured during the junction elongation[23] that exhibit peaks at $G \approx N \cdot G_0$, $N = 1, 2, \ldots$ However, the variation of peak shapes cannot be attributed to different environments.[23,40]

To summarize, we evaluated the effect of the environmental humidity on the adhesion in contacts formed between a gold surface and a gold-covered AFM probe. Our results demonstrate a clear correlation between the breaking forces of a gold nanojunction F_{adh} and the electric conductance of the junction before breaking G_{end}. The latter is related to the number of gold atoms in the thinnest part of a nanojunction and thus indirectly reflects the geometry of the junctions. For thick junctions with conductance $G_{end} > 20G_0$, the adhesion force behaves as a linear function of G_{end} independently of the humidity. On the other hand, "thin" junctions with conductance $G_{end} < 15G_0$ were stabilized by the presence of adsorbed water and only formed if the RH exceeded 14%. The breaking force of such junctions, 10−15 nN, was higher than that in dry atmosphere. We associate the difference to the contribution of the capillary force exerted by the water neck formed between the probe and the sample.

EXPERIMENTAL METHODS

We employed a CSAFM setup based on the PicoPlus 5500 SPM system (Agilent Technologies)[28] and AFM probes of the PPP-NCSTAu type (Nanosensors, nominal tip radius <50 nm) with a spring constant of 7−9 $N \cdot m^{-1}$. The probe was moved with a rate of 1000 $nm \cdot s^{-1}$. Unless stated otherwise, the experimental details were the same as those in ref 28. Atomically flat Au(111) substrates were fabricated and cleaned as described in ref 41. The humidity was maintained by continuously feeding dry and water-saturated argon (Carbagas 99.999%, < 3 ppm of H_2O) into the environmental chamber (Agilent Technologies) and varied by changing the flow rate ratio of the two streams. The RH was continuously monitored inside of the environmental chamber employing a Sensirion SHT11 digital humidity and temperature sensor. The sensor had the accuracy of 3% (with respect to the measured value) in the RH ranges of 20−80 and 3−5% at a RH below 20%.

AUTHOR INFORMATION

Corresponding Author

*E-mail: ilya.pobelov@dcb.unibe.ch.

Notes

The authors declare no competing financial interest.

ACKNOWLEDGMENTS

This work was supported by the Swiss National Science Foundation (200020_144471, NFP 62, Sinergia CRSII2 126969/1), the Swiss Commission for Technology and Innovation (13696.1), COST Action TD 1002, OTKA (105735), the bilateral mobility program of HAS (SNK-61/2013), and Sciex (10.209).

REFERENCES

(1) Adamson, A. W.; Gast, A. P. *Physical Chemistry of Surfaces*, 6th ed.; Wiley: New York, 1997.
(2) Verdaguer, A.; Sacha, G. M.; Bluhm, H.; Salmeron, M. Molecular Structure of Water at Interfaces: Wetting at the Nanometer Scale. *Chem. Rev.* **2006**, *106*, 1478−1510.
(3) Israelachvili, J. N. *Intermolecular and Surface Forces*, 3rd ed.; Elsevier Academic Press: New York, 2011.
(4) Cappella, B.; Dietler, G. Force−Distance Curves by Atomic Force Microscopy. *Surf. Sci. Rep.* **1999**, *34*, 1−104.
(5) Butt, H.-J.; Cappella, B.; Kappl, M. Force Measurements with the Atomic Force Microscope: Technique, Interpretation and Applications. *Surf. Sci. Rep.* **2005**, *59*, 1−152.
(6) Drelich, J., Mittal, K. L., Eds. *Atomic Force Microscopy in Adhesion Studies*; CRC Press: Boca Raton, FL, 2005.
(7) Weisenhorn, A. L.; Hansma, P. K.; Albrecht, T. R.; Quate, C. F. Forces in Atomic Force Microscopy in Air and Water. *Appl. Phys. Lett.* **1989**, *54*, 2651−2653.
(8) Thundat, T.; Zheng, X.-Y.; Chen, G.; Warmack, R. Role of Relative Humidity in Atomic Force Microscopy Imaging. *Surf. Sci.* **1993**, *294*, L939−L943.
(9) Binggeli, M.; Mate, C. M. Influence of Capillary Condensation of Water on Nanotribology Studied by Force Microscopy. *Appl. Phys. Lett.* **1994**, *65*, 415−417.
(10) Hu, J.; Xiao, X. D.; Ogletree, D. F.; Salmeron, M. Imaging the Condensation and Evaporation of Molecularly Thin Films of Water with Nanometer Resolution. *Science* **1995**, *268*, 267−269.
(11) Xu, L.; Lio, A.; Hu, J.; Ogletree, D. F.; Salmeron, M. Wetting and Capillary Phenomena of Water on Mica. *J. Phys. Chem. B* **1998**, *102*, 540−548.
(12) Song, M.-B.; Jang, J.-M.; Bae, S.-E.; Lee, C.-W. Charge Transfer through Thin Layers of Water Investigated by STM, AFM, and QCM. *Langmuir* **2002**, *18*, 2780−2784.
(13) Weeks, B. L.; Vaughn, M. W.; DeYoreo, J. J. Direct Imaging of Meniscus Formation in Atomic Force Microscopy Using Environmental Scanning Electron Microscopy. *Langmuir* **2005**, *21*, 8096−8098.
(14) Xu, K.; Cao, P.; Heath, J. R. Graphene Visualizes the First Water Adlayers on Mica at Ambient Conditions. *Science* **2010**, *329*, 1188−1191.
(15) Xiao, X.; Qian, L. Investigation of Humidity-Dependent Capillary Force. *Langmuir* **2000**, *16*, 8153−8158.
(16) Jones, R.; Pollock, H. M.; Cleaver, J. A. S.; Hodges, C. S. Adhesion Forces between Glass and Silicon Surfaces in Air Studied by AFM: Effects of Relative Humidity, Particle Size, Roughness, and Surface Treatment. *Langmuir* **2002**, *18*, 8045−8055.
(17) Farshchi-Tabrizi, M.; Kappl, M.; Cheng, Y.; Gutmann, J.; Butt, H.-J. On the Adhesion between Fine Particles and Nanocontacts: An Atomic Force Microscope Study. *Langmuir* **2006**, *22*, 2171−2184.
(18) Xu, Q.; Li, M.; Niu, J.; Xia, Z. Dynamic Enhancement in Adhesion Forces of Microparticles on Substrates. *Langmuir* **2013**, *29*, 13743−13749.
(19) Zarate, N. V.; Harrison, A. J.; Litster, J. D.; Beaudoin, S. P. Effect of Relative Humidity on Onset of Capillary Forces for Rough Surfaces. *J. Colloid Interface Sci.* **2013**, *411*, 265−272.
(20) Guckenberger, R.; Heim, M.; Cevc, G.; Knapp, H.; Wiegräbe, W.; Hillebrand, A. Scanning Tunneling Microscopy of Insulators and Biological Specimens Based on Lateral Conductivity of Ultrathin Water Films. *Science* **1994**, *266*, 1538−1540.
(21) Guo, L.; Jiang, H.-B.; Shao, R.-Q.; Zhang, Y.-L.; Xie, S.-Y.; Wang, J.-N.; Li, X.-B.; Jiang, F.; Chen, Q.-D.; Zhang, T.; et al. Two-Beam-Laser Interference Mediated Reduction, Patterning and Nanostructuring of Graphene Oxide for the Production of a Flexible Humidity Sensing Device. *Carbon* **2012**, *50*, 1667−1673.
(22) Xu, B.; Xiao, X.; Tao, N. J. Measurements of Single-Molecule Electromechanical Properties. *J. Am. Chem. Soc.* **2003**, *125*, 16164−16165.
(23) Agraït, N.; Yeyati, A. L.; van Ruitenbeek, J. M. Quantum Properties of Atomic-Sized Conductors. *Phys. Rep.* **2003**, *377*, 81−279.
(24) Li, C.; Mishchenko, A.; Pobelov, I.; Wandlowski, T. Charge Transport with Single Molecules — An Electrochemical Approach. *Chimia* **2010**, *64*, 383−390.

(25) Aradhya, S. V.; Venkataraman, L. Single-Molecule Junctions beyond Electronic Transport. *Nat. Nanotechnol.* **2013**, *8*, 399−410.
(26) Sun, L.; Diaz-Fernandez, Y. A.; Gschneidtner, T. A.; Westerlund, F.; Lara-Avilab, S.; Moth-Poulsen, K. Single-Molecule Electronics: From Chemical Design to Functional Devices. *Chem. Soc. Rev.* **2014**, *43*, 7378−7411.
(27) Rubio-Bollinger, G.; Bahn, S. R.; Agraït, N.; Jacobsen, K. W.; Vieira, S. Mechanical Properties and Formation Mechanisms of a Wire of Single Gold Atoms. *Phys. Rev. Lett.* **2001**, *87*, 026101.
(28) Pobelov, I. V.; Mészáros, G.; Yoshida, K.; Mishchenko, A.; Gulcur, M.; Bryce, M. R.; Wandlowski, T. An Approach to Measure Electromechanical Properties of Atomic and Molecular Junctions. *J. Phys.: Condens. Matter* **2012**, *24*, 164210.
(29) Nef, C.; Frederix, P. L. T. M.; Brunner, J.; Schönenberger, C.; Calame, M. Force-Conductance Correlation in Individual Molecular Junctions. *Nanotechnology* **2012**, *23*, 365201.
(30) Pobelov, I. V.; Mohos, M.; Yoshida, K.; Kolivoska, V.; Avdic, A.; Lugstein, A.; Bertagnolli, E.; Leonhardt, K.; Denuault, G.; Gollas, B.; et al. Electrochemical Current-Sensing Atomic Force Microscopy in Conductive Solutions. *Nanotechnology* **2013**, *24*, 115501.
(31) Marszalek, P. E.; Greenleaf, W. J.; Li, H.; Oberhauser, A. F.; Fernandez, J. M. Atomic Force Microscopy Captures Quantized Plastic Deformation in Gold Nanowires. *Proc. Natl. Acad. Sci. U.S.A.* **2000**, *97*, 6282−6286.
(32) Frei, M.; Aradhya, S. V.; Koentopp, M.; Hybertsen, M. S.; Venkataraman, L. Mechanics and Chemistry: Single Molecule Bond Rupture Forces Correlate with Molecular Backbone Structure. *Nano Lett.* **2011**, *11*, 1518−1523.
(33) Aradhya, S. V.; Frei, M.; Halbritter, A.; Venkataraman, L. Correlating Structure, Conductance, and Mechanics of Silver Atomic-Scale Contacts. *ACS Nano* **2013**, *7*, 3706−3712.
(34) Bussian, D. A.; O'Dea, J. R.; Metiu, H.; Buratto, S. K. Nanoscale Current Imaging of the Conducting Channels in Proton Exchange Membrane Fuel Cells. *Nano Lett.* **2007**, *7*, 227−232.
(35) Aleksandrova, E.; Hiesgen, R.; Friedrich, K. A.; Roduner, E. Electrochemical Atomic Force Microscopy Study of Proton Conductivity in a Nafion Membrane. *Phys. Chem. Chem. Phys.* **2007**, *9*, 2735−2743.
(36) Kang, Y.; Kwon, O.; Xie, X.; Zhu, D.-M. Conductance Mapping of Proton Exchange Membranes by Current Sensing Atomic Force Microscopy. *J. Phys. Chem. B* **2009**, *113*, 15040−15046.
(37) He, Q.; Kusoglu, A.; Lucas, I. T.; Clark, K.; Weber, A. Z.; Kostecki, R. Correlating Humidity-Dependent Ionically Conductive Surface Area with Transport Phenomena in Proton-Exchange Membranes. *J. Phys. Chem. B* **2011**, *115*, 11650−11657.
(38) Hara, M.; Hattori, D.; Inukai, J.; Bae, B.; Hoshi, T.; Hara, M.; Miyatake, K.; Watanabe, M. Imaging Individual Proton-Conducting Spots on Sulfonated Multiblock-Copolymer Membrane under Controlled Hydrogen Atmosphere by Current-Sensing Atomic Force Microscopy. *J. Phys. Chem. B* **2013**, *117*, 3892−3899.
(39) Abellán, J.; Chicón, R.; Arenas, A. Properties of Nanowires in Air: Controlled Values of Conductance. *Surf. Sci.* **1998**, *418*, 493−501.
(40) Pobelov, I. V. *Electron Transport Studies — An Electrochemical Scanning Tunneling Microscopy Approach*. Ph.D. Thesis, RWTH Aachen, Aachen, Germany, 2008; Chapter 5.
(41) Kolivoška, V.; Mohos, M.; Pobelov, I. V.; Rohrbach, S.; Yoshida, K.; Hong, W.; Fu, Y.; Moreno-García, P.; Mészáros, G.; Broekmann, P.; et al. Electrochemical Control of a Non-Covalent Binding between Ferrocene and *β*-Cyclodextrin. *Chem. Commun.* **2014**, *50*, 11757−11759.